

## Article

# Effect of the Metal Deposition Order on Structural, Electronic and Catalytic Properties of TiO<sub>2</sub>-Supported Bimetallic Au-Ag Catalysts in 1-Octanol Selective Oxidation

Yulia Kotolevich <sup>1</sup>, Ekaterina Pakrieva <sup>2,3</sup>, Ekaterina Kolobova <sup>2</sup>, Mario H. Farías <sup>1</sup>, Nina Bogdanchikova <sup>1</sup>, Vicente Cortés Corberán <sup>3</sup>, Daria Pichugina <sup>4</sup>, Nadezhda Nikitina <sup>4</sup>, Sónia A. C. Carabineiro <sup>5</sup> and Alexey Pestryakov <sup>2,6,\*</sup>

- <sup>1</sup> Centro de Nanociencias y Nanotecnología, Universidad Nacional Autónoma de México, Ensenada 22800, Mexico; julia.kotolevich@gmail.com (Y.K.); mario@cnyn.unam.mx (M.H.F.); nina@cnyn.unam.mx (N.B.)
  - <sup>2</sup> Research School of Chemistry & Applied Biomedical Sciences, National Research Tomsk Polytechnic University, 634050 Tomsk, Russia; epakrieva@mail.ru (E.P.); ekaterina\_kolobova@mail.ru (E.K.)
  - <sup>3</sup> Instituto de Catálisis y Petroleoquímica, Consejo Superior de Investigaciones Científicas, Marie Curie 2, 28049 Madrid, Spain; vcortes@icp.csic.es
  - <sup>4</sup> Department of Chemistry, Lomonosov Moscow State University, 1-3 Leninskiye Gory, GSP-1, 119991 Moscow, Russia; dashapi@mail.ru (D.P.); nnikitina1719@gmail.com (N.N.)
  - <sup>5</sup> LAQV-REQUIMTE, Department of Chemistry, NOVA School of Science and Technology, Universidade NOVA de Lisboa, 2829-516 Caparica, Portugal; sonia.carabineiro@fct.unl.pt
  - <sup>6</sup> Research Department, Sevastopol State University, 299053 Sevastopol, Russia
- \* Correspondence: pestryakov2005@yandex.ru



**Citation:** Kotolevich, Y.; Pakrieva, E.; Kolobova, E.; Farías, M.H.;

Bogdanchikova, N.; Cortés Corberán, V.; Pichugina, D.; Nikitina, N.; Carabineiro, S.A.C.; Pestryakov, A. Effect of the Metal Deposition Order on Structural, Electronic and Catalytic Properties of TiO<sub>2</sub>-Supported Bimetallic Au-Ag Catalysts in 1-Octanol Selective Oxidation. *Catalysts* **2021**, *11*, 799. <https://doi.org/10.3390/catal11070799>

Academic Editor: Leonarda Francesca Liotta

Received: 1 June 2021  
Accepted: 26 June 2021  
Published: 30 June 2021

**Publisher's Note:** MDPI stays neutral with regard to jurisdictional claims in published maps and institutional affiliations.



**Copyright:** © 2021 by the authors. Licensee MDPI, Basel, Switzerland. This article is an open access article distributed under the terms and conditions of the Creative Commons Attribution (CC BY) license (<https://creativecommons.org/licenses/by/4.0/>).

**Abstract:** Au and Ag were deposited on TiO<sub>2</sub> modified with Ce, La, Fe or Mg in order to obtain bimetallic catalysts to be used for liquid-phase oxidation of 1-octanol. The effects of the deposition order of gold and silver, and the nature of the support modifying additives and redox pretreatments on the catalytic properties of the bimetallic Au-Ag catalysts were studied. Catalysts were characterized by low-temperature nitrogen adsorption-desorption, energy dispersive spectroscopy, X-ray diffraction, X-ray photoelectron spectroscopy, high-resolution transmission electron microscopy and ultraviolet-visible diffuse reflectance spectroscopy. It was found that pretreatments with hydrogen and oxygen at 300 °C significantly decreased the activity of AuAg catalysts (silver was deposited first) and had little effect on the catalytic properties of AgAu samples (gold was deposited first). The density functional theory method demonstrated that the adsorption energy of 1-octanol increased for all positively charged Au<sub>x</sub>Ag<sub>y</sub><sup>q</sup> (x + y = 10, with a charge of q = 0 or +1) clusters compared with the neutral counterparts. Lanthanum oxide was a very effective promoter for both monometallic and bimetallic gold and silver catalysts in the studied process.

**Keywords:** gold; silver; bimetallic catalysts; 1-octanol oxidation

## 1. Introduction

Gold nanoparticles are unique catalysts for many low-temperature processes [1,2]. The majority of the reported works deal with the tuning of the gold particle size, support modification and the pretreatment conditions [1,2]. Many research groups continue to look for ways to further improve the efficiency of nanogold catalysts. One of these methods is the synthesis of bimetallic systems consisting of two catalytically active metals, as well as the addition of modifying additives made of various compounds. The physical and chemical properties of alloys often differ from those of monometallic particles and largely vary with composition and particle sizes [3,4]. Thus, gold-based catalysts' properties could be improved by modification with a second metal with stronger affinity to O<sub>2</sub> than gold has. It has been reported that several Au-containing bimetallic catalysts like Au-Cu [4,5], Au-Ag [6–16], Au-Pt [17,18] and Au-Pd [18–20] demonstrated an improvement in catalytic

properties in a variety of reactions. Among them, Ag (a metal of the IB group of the periodic table, just like Au) has similar cell parameters and high affinity for Au atoms, and can easily form homogeneous bimetallic Au-Ag alloys without phase segregation [21]. Silver nanoparticles are also active catalysts for the low-temperature oxidation of CO and organic substances [22–24]. The transfer of electron density between metals or modifiers is one of the reasons for the increased stability of gold in bimetallic and modified catalysts [25].

Synergistic effects and improved activities by Au-Ag alloying have been obtained, particularly for low-temperature CO oxidation [11,25–35]. In terms of alcohol oxidation, Wittstock et al. reported the highly efficient oxidative coupling of methanol on nanoporous Au-Ag alloys due to regulation of the availability of reactive oxygen species on Ag [36,37]. Octanol oxidation is an important yet still not much studied model reaction for a series of liquid-phase oxidation processes of gold. Just a few works studying gold catalysts in octanol oxidation are known [38]. In our group, modified Au/M/TiO<sub>2</sub> catalysts, where M is La, Ce, Fe or Mg oxide, were developed and used for 1-octanol oxidation [39,40]. These materials were the prototypes of one of the most efficient catalysts for low-temperature CO oxidation [41–43]. Thus, we thought that the Au-Ag alloys might be an interesting alternative to improve the catalytic performance for 1-octanol oxidation. We started our investigation with Au-Ag catalysts earlier [44], but we did not compare the properties of the catalysts with a different metal deposition order.

The catalytic activity of the bimetallic gold–silver catalysts was found to depend on the support material and catalyst preparation method [45]. However, when AgNO<sub>3</sub> and HAuCl<sub>4</sub> were used as catalyst precursors, the formation of insoluble halide precipitations, such as AgCl, occurred, which led to the contamination of alloy NPs and complications in alloy composition control [46–48]. One of the methods to avoid the Cl contamination is to vary the order of the components' deposition [44].

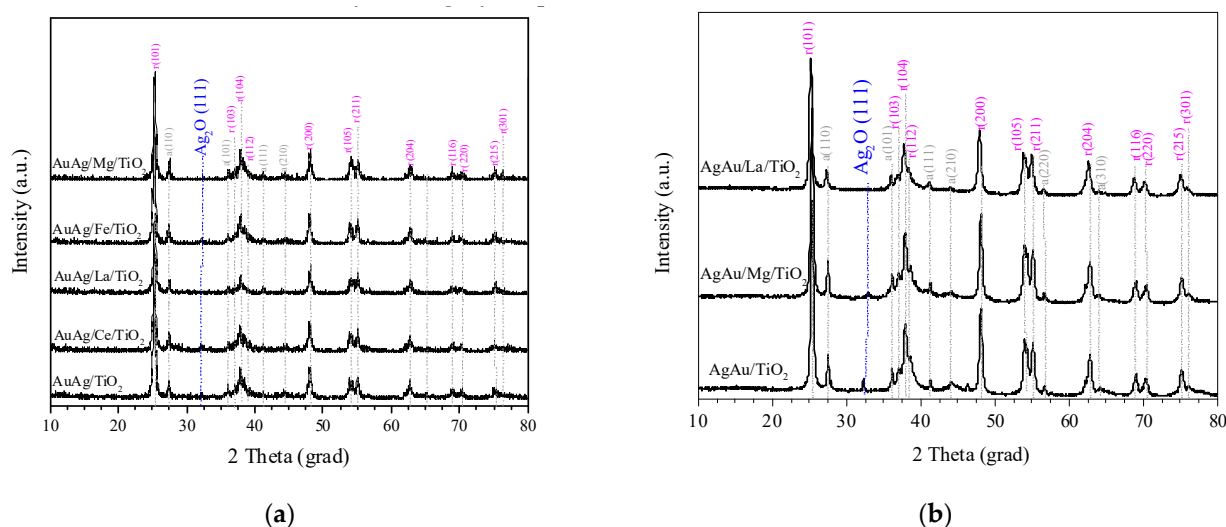
In this work, gold and silver were deposited on TiO<sub>2</sub> modified with Ce, La, Fe or Mg metal oxides (M), in different orders: silver deposited first and then Au (AuAg/M/TiO<sub>2</sub>), or Au was deposited first and then Ag (AgAu/M/TiO<sub>2</sub>). We aimed to investigate the effect of the deposition order of gold and silver on the support, and the influence of modifying additives and redox pretreatments on the change in the catalytic, structural and electronic properties of these bimetallic Au-Ag catalysts for liquid-phase oxidation of 1-octanol.

## 2. Results and Discussion

### 2.1. Characterization Results

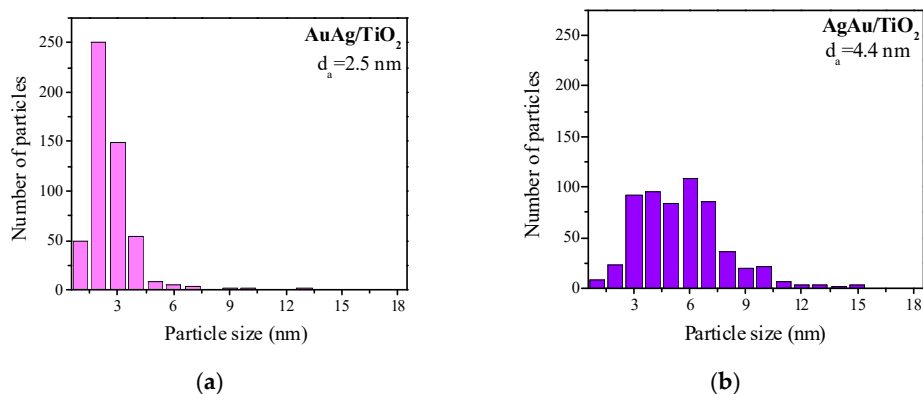
The elemental analysis results demonstrated that the real gold and silver loadings obtained were similar to the nominal values (Table S1). Table S1 also summarizes the specific surface area ( $S_{\text{BET}}$ ) of the catalysts and their corresponding supports. Thus, the textural properties of the studied catalysts were not so different from each other.

Figure 1 shows the X-ray diffraction (XRD) diffractograms of selected samples. Besides the narrow diffraction lines corresponding to the support (anatase—gray color; rutile—pink color), the peak of Ag<sub>2</sub>O (blue color) was detected for AuAg supported on TiO<sub>2</sub> and Ce/TiO<sub>2</sub>, and for AgAu supported on TiO<sub>2</sub> and Mg/TiO<sub>2</sub>, with crystallite sizes of around 5–8 nm. According to the catalyst preparation method (see Materials and Methods), silver should be deposited as Ag<sub>2</sub>O. The fact that only AuAg/TiO<sub>2</sub>, AuAg/Ce/TiO<sub>2</sub>, AgAu/TiO<sub>2</sub> and AgAu/Mg/TiO<sub>2</sub> showed a crystalline phase of silver oxide while the Ag contents in these samples had no significant difference as compared with the others (Table S1) might be due to the metal–support interaction features during synthesis (stabilization of Ag<sub>2</sub>O particles). The absence of the peaks of gold-containing phases suggests either a non-crystal structure of gold and/or the existence of Au species with a size below 1–2 nm. The absence of well-defined lines corresponding to the support modifiers shows that they are highly dispersed on the TiO<sub>2</sub> surface.



**Figure 1.** XRD patterns of AuAg (a) and AgAu (b) catalysts. Diffraction lines corresponding to TiO<sub>2</sub> anatase phase are marked with “a” (in gray color), while those corresponding to rutile have “r” (magenta color) with their corresponding Miller indexes. Samples were studied after a reduction in H<sub>2</sub> at 300 °C for 1 h.

Figure 2 displays the particle size distribution obtained from high-resolution transmission electron microscopy (HRTEM) images (Figure S1) of the H<sub>2</sub>-reduced samples. AuAg samples are represented as pink histograms and AgAu samples as purple ones. All the studied samples were characterized by a broad distribution of particle sizes, the majority within the 1–10 nm interval. It is interesting to note that AuAg supported on unmodified TiO<sub>2</sub> showed the narrowest particle size distribution and the smallest average particle size of 2.5 nm, while AuAg on modified supports showed broader particle size distributions. Regarding the AgAu series, TiO<sub>2</sub> support modification with Ce and Mg did not show any effect on the particle size distribution: for AgAu/TiO<sub>2</sub> (Figure 2b), AgAu/Mg/TiO<sub>2</sub> (Figure 2f) and AgAu/Ce/TiO<sub>2</sub> (Figure 2h), the average size was 4.4 nm and the particle size distribution interval was 1–6 nm. La and Fe as modifiers of TiO<sub>2</sub> in the AgAu series made the particle size distribution narrower than on unmodified titania. Both AgAu and AuAg on TiO<sub>2</sub> modified with La demonstrated close average sizes (3.2 and 3.3 nm, respectively) and a similar interval of the size distribution (1–6 nm), which might mean that the deposition order (AuAg or AgAu) is not important for La/TiO<sub>2</sub>. Analyzing both the XRD and HRTEM results allowed us to conclude that relatively large (2.5–6.7 nm) unstructured particles were formed for both deposition orders.



**Figure 2.** Cont.

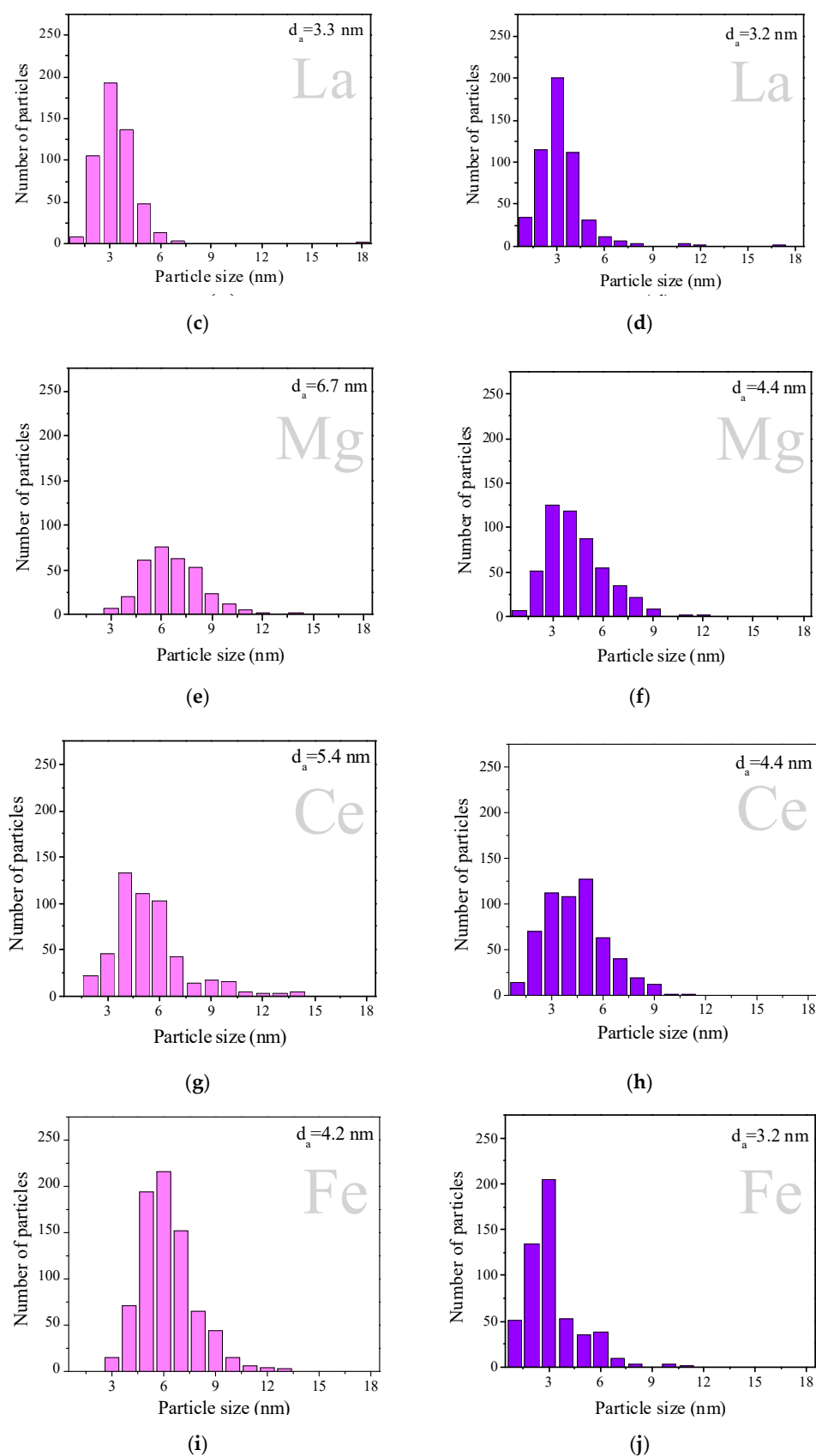


**Figure 2.** Particles size distribution of AuAg (pink) and AgAu (purple) catalysts on different supports: TiO<sub>2</sub> (a,b), La/TiO<sub>2</sub> (c,d), Mg/TiO<sub>2</sub> (e,f), Ce/TiO<sub>2</sub> (g,h) and Fe/TiO<sub>2</sub> (i,j). Samples were studied after reduction in H<sub>2</sub> at 300 °C for 1 h. Some previously reported results concerning AuAg samples are included for comparison, reprinted from [44] (copyright 2017), with permission from EUREKA SCIENCE.

In order to study the metal species' nature and determine whether the catalysts included sub-nanometer species or not, several physicochemical methods of characterization were applied.

Ultraviolet–visible diffuse reflectance spectroscopy (UV-vis DRS) allows the detection of sub-nanometer Au and Ag clusters (<1 nm) by the presence of absorption peaks at <400 nm [49–51]. In our work, since all samples had strong absorption below 420 nm, given the band gap excitation of TiO<sub>2</sub>, it was not possible to assess the information about sub-nanometer clusters of Au and Ag (Figure 3). The spectra of monometallic Ag catalysts supported on La/TiO<sub>2</sub> and Mg/TiO<sub>2</sub> showed the tail of the peak above 400 nm, which could correspond to nanoparticles of Ag<sub>n</sub><sup>δ+</sup> absorbing at 370–380 nm [52]. At the same time, the spectra of monometallic silver samples supported on Ce- or Fe-modified and unmodified TiO<sub>2</sub> demonstrated weak and wide unstructured absorption at 400–650 nm, which corresponded to the silver metal nanoparticles [53–55].

Monometallic gold supported on La-, Fe-, and Mg-modified titania surfaces demonstrated weak and broad unstructured absorption at 400–900 nm, confirming the formation of non-spherical gold nanoparticles, while Au/Ce/TiO<sub>2</sub> and Au/TiO<sub>2</sub> demonstrated peaks with a maximum at 520–570 nm. It is known that the maximum of this DRS adsorption peak is highly dependent on the particles' size and shape, and the aggregation of Au NPs, and leads to a shift in the surface plasmon resonance band from 529 to 660 nm [56–59]. All bimetallic catalysts exhibited a peak with a maximum at 500–700 nm, very similar for both AuAg and AgAu samples on each support. This peak was located at the wavelength range corresponding to Au surface plasmon [60,61]. We may conclude that the metallic/plasmon species of all the studied catalysts had a similar nature/structure. The difference among them should be found in the sub-nanoscale. The adsorption at 495 nm for Fe-modified samples (Figure 2b) is attributed to O–Fe charge transfers involving octahedral Fe(III) [62]. It should also be noted that in the spectra of most of the modified monometallic samples (except Au/Ce/TiO<sub>2</sub>), the plasmon signals are much less pronounced compared with those of bimetallic ones.

X-ray photoelectron spectroscopy (XPS) was applied to investigate the electronic states of the gold surface. Figure 4 shows the results of the Au (Figure 4a), AuAg (Figure 4b) and AgAu samples (Figure 4c). The interpretation of the XPS data based on the literature [64–68] is presented in Table 1. The XPS peaks corresponding to possible oxidation states overlap, and thus the peaks must be resolved by fitting. The results presented represent one solution for resolving the peaks, and the true oxidation states may be different.

Au 4f peak doublets showing large widths were subjected to a resolving process. Based on the resolving results, we supposed the existence of five gold surface states and that the metallic state was predominant in all the studied samples. It can be seen that the XPS data of AuAg are closer to those of monometallic Au than those of AgAu when the electronic stages of gold and their contributions are compared. All AgAu samples were characterized by a minimal number (1 or 2) of gold electronic states and all of them are reduced species, except for 5% of oxidized gold in AgAu/TiO<sub>2</sub>. On the contrary, monometallic and AuAg samples demonstrated up to four different gold species, and the contribution of the oxidized ones represents 19–45%. The largest diversity of gold electronic species is shown for Fe-modified samples.

Figure 5 shows the XPS spectra of the Ag 3d<sub>5/2</sub> lines of the Ag (Figure 5a), AuAg (Figure 5b) and AgAu (Figure 5c) samples. The interpretation of the spectra made in accordance with the literature data [69–71] is shown in Table 2.

Ag 3d<sub>5/2</sub> peaks also required resolution in all cases, due to their large widths. Just like with gold, the XPS data for AuAg were closer to those of monometallic samples than those of AgAu, and the AgAu catalyst series demonstrated minimal diversity in the electronic states of silver. It also can be seen that the silver electronic state was much more affected by additives and deposition order than gold. Since silver was deposited as Ag<sub>2</sub>O and all samples were treated with H<sub>2</sub> at 300 °C, it was expected that reduced states of silver were present. However, besides the metallic state (gray peak) found in most of the presented

spectra, a large contribution of  $\text{Ag}^+$  (pink peak) was observed, which could be explained by the stabilization of silver oxide through interaction with the support. It is interesting to note that when Fe and Ce modifiers were present, and only then, the formation of  $\text{Ag}^+$  (green peak) was detected. It could have been due to a peculiar interaction between silver and these electron-acceptor modifiers. Around half of the studied samples showed the formation of small silver clusters (purple peaks): The Ag and AuAg catalysts modified with La, Mg and Fe and also AgAu/TiO<sub>2</sub>. It is interesting to note that the contribution of the silver small clusters varied drastically, from 5% up to 80% (Table 2), but small clusters represented 100% of the silver in AuAg/La/TiO<sub>2</sub>.

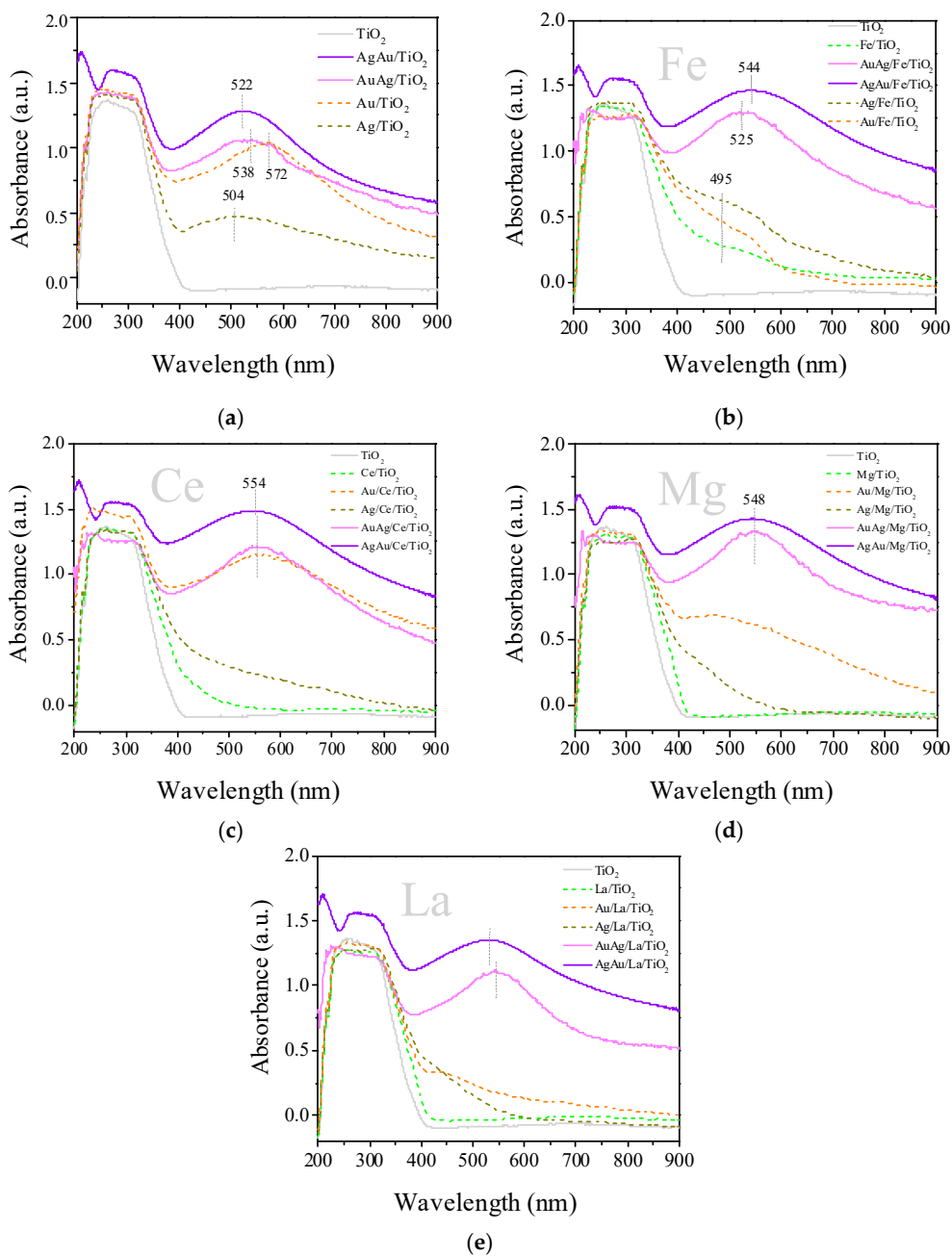


**Figure 3.** Diffuse reflectance UV-vis spectra of samples on different supports: TiO<sub>2</sub> (a), Fe/TiO<sub>2</sub> (b), Ce/TiO<sub>2</sub> (c), Mg/TiO<sub>2</sub> (d) and La/TiO<sub>2</sub> (e). Samples were studied after reduction in H<sub>2</sub> at 300 °C for 1 h. Previously reported data for Au/M/TiO<sub>2</sub> catalysts are reprinted from [39,40] (copyright 2004), with permission from Elsevier. Data for Ag/M/TiO<sub>2</sub> were adapted from [63].

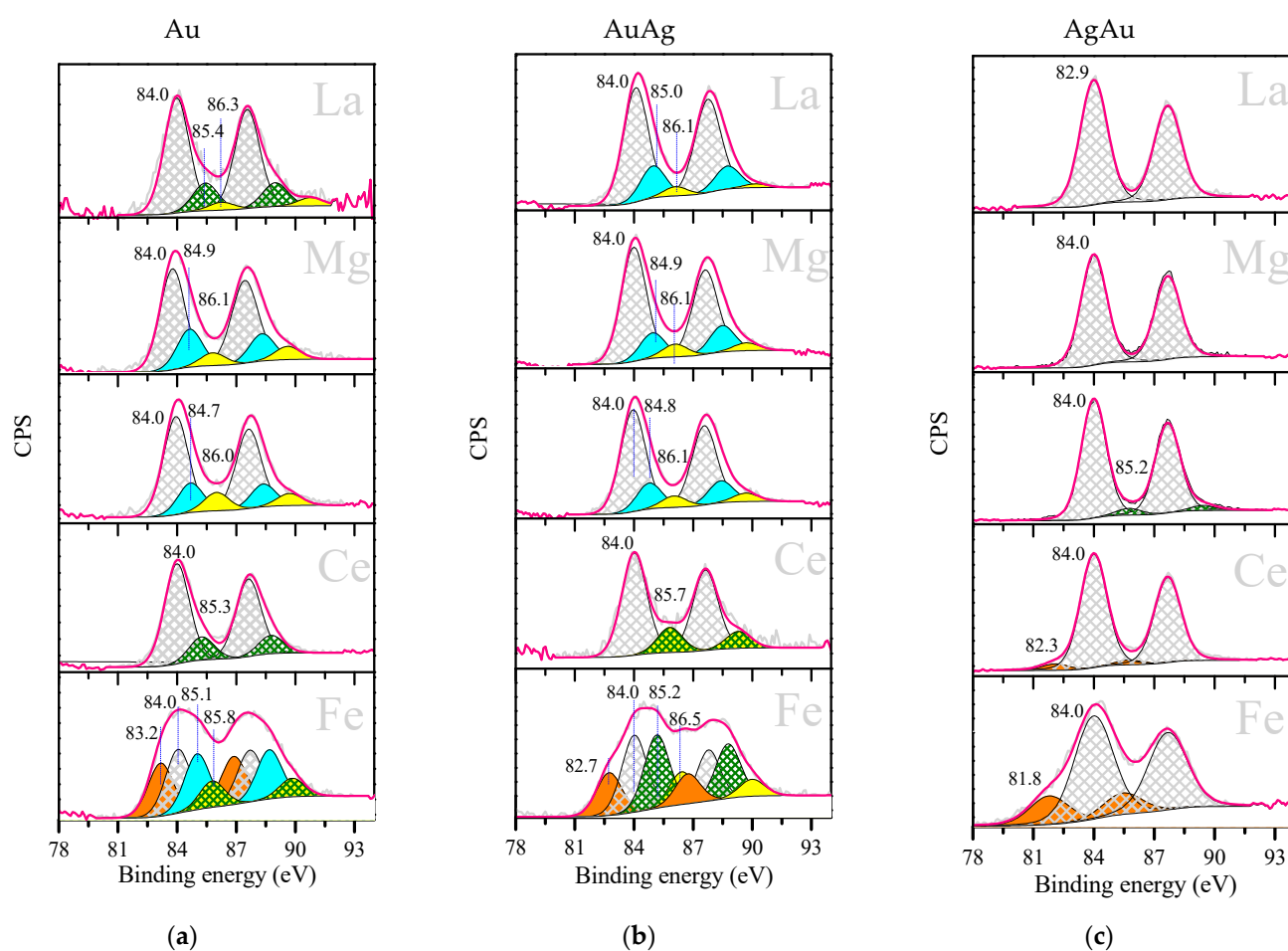


**Figure 4.** Au  $4f_{7/2}$  XPS for Au (a), AuAg (b), AgAu (c) catalysts supported on M/TiO<sub>2</sub>, where M is La, Mg, Ce or Fe. Samples were studied after reduction in H<sub>2</sub> at 300 °C for 1 h. Previously reported XPS data for Au/M/TiO<sub>2</sub> catalysts are included for comparison, reprinted from [39,40] (copyright 2004), with permission from Elsevier.

**Table 1.** Binding energies (BE) of different gold electronic states (eV) and their relative content (%), indicated in parentheses. Data for Au/M/TiO<sub>2</sub> catalysts are reprinted from [39,40] (copyright 2004), with permission from Elsevier.

Catalysts	Au <sub>n</sub> <sup>δ-</sup>	Au <sup>0</sup>	Au <sup>+</sup>	Au <sup>3+</sup>
	≤83.6 eV	~84 eV	~85–85.5 eV	~86–87 eV
Au/La/TiO <sub>2</sub>	-	84.0 (76%)	85.4 (18%)	86.3 (6%)
AuAg/La/TiO <sub>2</sub>	-	84.0 (71%)	85.0 (23%)	86.1 (6%)
AgAu/La/TiO <sub>2</sub>	-	84.0 (100%)	-	-
Au/Mg/TiO <sub>2</sub>	-	84.0 (68%)	84.9 (23%)	86.1 (9%)
AuAg/Mg/TiO <sub>2</sub>	-	84.0 (73%)	84.9 (19%)	86.1 (8%)
AgAu/Mg/TiO <sub>2</sub>	-	84.0 (100%)	-	-
Au/TiO <sub>2</sub>	-	84.0 (68%)	84.7 (20%)	86.0 (12%)
AuAg/TiO <sub>2</sub>	-	84.0 (73%)	84.8 (19%)	86.1 (8%)
AgAu/TiO <sub>2</sub>	-	83.1 (95%)	85.2 (5%)	-
Au/Ce/TiO <sub>2</sub>	-	84.0 (81%)	85.3 (19%)	-
AuAg/Ce/TiO <sub>2</sub>	-	84.0 (81%)	85.7 (19%)	-
AgAu/Ce/TiO <sub>2</sub>	82.3 (5%)	84.0 (95%)	-	-
Au/Fe/TiO <sub>2</sub>	83.1 (28%)	84.0 (32%)	85.0 (29%)	85.8 (11%)
AuAg/Fe/TiO <sub>2</sub>	82.7 (18%)	84.0 (35%)	85.2 (33%)	86.5 (14%)
AgAu/Fe/TiO <sub>2</sub>	81.8 (22%)	84.0 (78%)	-	-

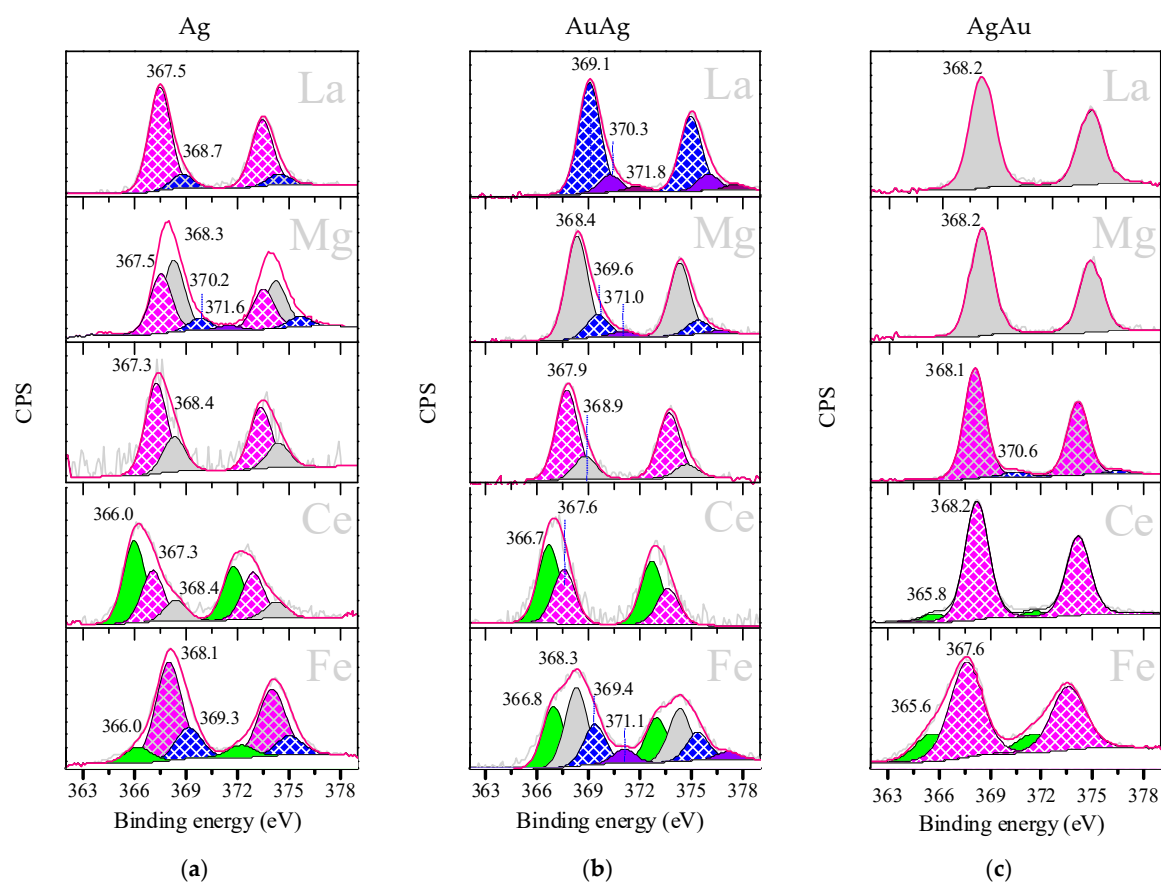


**Figure 5.** Ag  $3d_{5/2}$  XPS for Ag (a), AuAg (b) and AgAu (c) catalysts supported on M/TiO<sub>2</sub>, where M is La, Mg, Ce or Fe. Samples were studied after reduction in H<sub>2</sub> at 300 °C for 1 h. Some previously reported XPS results of Ag-based samples are shown in (a) [63].

**Table 2.** BE of different silver electronic states (eV) and their relative content (%), indicated in parenthesis. Data for Ag/M/TiO<sub>2</sub> were adapted from [63].

Catalyst	Ag <sup>+</sup>	Ag <sup>δ+</sup>	Ag <sup>0</sup>	Ag Clusters <2 nm
	364.0–366.2	367.4–367.9	368.1–368.4	>369.0
Ag/La/TiO <sub>2</sub>	-	367.5 (84%)	368.7 (16%)	-
AuAg/La/TiO <sub>2</sub>	-	-	-	369.1 (80%) 370.3 (15%) 371.8 (5%)
AgAu/La/TiO <sub>2</sub>	-	-	368.2 (100%)	-
Ag/Mg/TiO <sub>2</sub>	-	367.5 (40%)	368.3 (47%)	369.9 (9%) 371.6 (4%)
AuAg/Mg/TiO <sub>2</sub>	-	-	368.4 (79%)	369.6 (17%) 371.0 (4%)
AgAu/Mg/TiO <sub>2</sub>	-	-	368.2 (100%)	-
Ag/TiO <sub>2</sub>	-	367.3 (80%)	368.4 (20%)	-
AuAg/TiO <sub>2</sub>	-	367.9 (81%)	368.9 (19%)	-
AgAu/TiO <sub>2</sub>	-	368.1 (95%)	-	370.6 (5%)
Ag/Ce/TiO <sub>2</sub>	366.0 (73%)	366.5 (19%)	367.8 (8%)	-
AuAg/Ce/TiO <sub>2</sub>	366.7 (61%)	367.6 (39%)	-	-
AgAu/Ce/TiO <sub>2</sub>	365.8 (7%)	367.4 (93%)	-	-
Ag/Fe/TiO <sub>2</sub>	366.0 (14%)	-	368.1 (65%)	369.3 (21%)
AuAg/Fe/TiO <sub>2</sub>	366.8 (32%)	-	368.3 (21%)	369.4 (40%) 371.1 (7%)
AgAu/Fe/TiO <sub>2</sub>	365.6 (20%)	367.6 (80%)	-	-

## 2.2. Catalytic Results

Figure 6 shows the results of the catalytic tests of 1-octanol oxidation for AuAg (Figure 6a) and AgAu catalysts (Figure 6b) supported on pristine and modified TiO<sub>2</sub> after different redox pretreatments. AuAg/La/TiO<sub>2</sub> was the most active catalyst for all kinds of pretreatment. In both groups, AuAg and AgAu, the catalytic activity decreased in the following support order: La/TiO<sub>2</sub> ≥ Mg/TiO<sub>2</sub> > TiO<sub>2</sub> > Ce/TiO<sub>2</sub> ≥ Fe/TiO<sub>2</sub>. Concerning the influence of pretreatment, for the AuAg series, the pretreatment drastically affected the catalytic activity. In most cases, H<sub>2</sub> pretreatment almost completely suppressed the catalytic activity of the samples (except for the La-modified one). O<sub>2</sub> pretreatment also reduced the activity but not to the same extent. For the samples with the other order of metal deposition (AgAu), the opposite effects were observed. In most cases, pretreatments had little effect on the activity of the catalysts or slightly increased it.

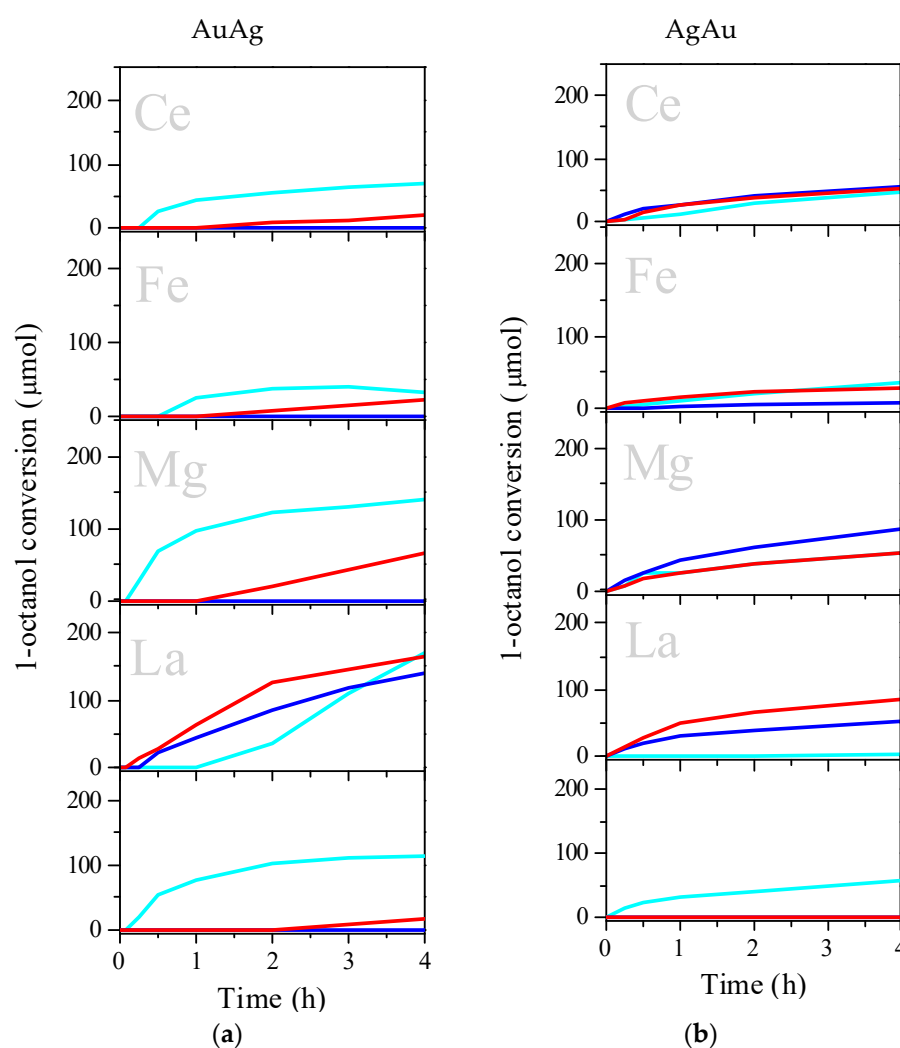


**Figure 6.** Effect of the metal deposition order on catalytic activity in 1-octanol oxidation: AuAg/M/TiO<sub>2</sub> (a) and AgAu/M/TiO<sub>2</sub> (b) for as prepared (light blue), H<sub>2</sub>-pretreated (blue) and O<sub>2</sub>-pretreated (red) samples. Reaction conditions: 0.1 M of 1-octanol in n-heptane; T = 80 °C; molar ratio octanol/Au = 100; no base added. Some previously reported results (a) are included for comparison, reprinted from [44] (copyright 2017), with permission from EUREKA SCIENCE.

Regarding selectivity of 1-octanol oxidation (Table 3), there are three possible products of this reaction: octanal (aldehyde), octyl octanoate (ester) and octanoic acid.

**Table 3.** Effect of the metal deposition order on the selectivity after 4 h of 1-octanol oxidation for AuAg/M/TiO<sub>2</sub> and AgAu/M/TiO<sub>2</sub>, where M is Ce, La, Fe or Mg oxide.

Catalyst	Selectivity, mol.%								
	Octanal			Octyl Octanoate			Octanoic Acid		
	as-prep.	H <sub>2</sub>	O <sub>2</sub>	as-prep.	H <sub>2</sub>	O <sub>2</sub>	as-prep.	H <sub>2</sub>	O <sub>2</sub>
AuAg/Ce/TiO <sub>2</sub>	86.5	0.0	75.9	7.0	0.0	24.8	6.5	0.0	0.0
AuAg/Fe/TiO <sub>2</sub>	100.0	0.0	76.3	0.0	0.0	23.8	0.0	0.0	0.0
AuAg/Mg/TiO <sub>2</sub>	82.1	0.0	62.1	-	0.0	31.9	7.9	0.0	6.0
AuAg/La/TiO <sub>2</sub>	52.7	83.1	34.6	47.3	14.0	61.2	0.0	2.9	4.1
AuAg/TiO <sub>2</sub>	93.5	0.0	71.3	0.0	0.0	28.7	6.5	0.0	0.0
AgAu/Ce/TiO <sub>2</sub>	92.6	95.8	95.3	7.4	4.2	4.7	0.0	0.0	0.0
AgAu/Fe/TiO <sub>2</sub>	92.2	100	91.2	7.8	0	8.8	0.0	0.0	0.0
AgAu/Mg/TiO <sub>2</sub>	93.9	94.2	94.3	6.1	5.8	5.7	0.0	0.0	0.0
AgAu/La/TiO <sub>2</sub>	100	91.9	86.3	0.0	8.1	13.7	0.0	0.0	0.0
AgAu/TiO <sub>2</sub>	93.2	0.0	100.0	6.8	0.0	0.0	0.0	0.0	0.0

For the majority of the studied catalysts, independently of the redox pretreatment, only aldehyde and ester were formed during the reaction, the predominant product being aldehyde, while acid was produced only in some cases on AuAg catalysts. The only exception was AuAg/La/TiO<sub>2</sub>: being the most active of the studied catalysts, it was able to provide deeper oxidation during 6 h of reaction; thus, the selectivity to octanal and to ester on as-prepared AuAg/La/TiO<sub>2</sub> was almost equal, while after O<sub>2</sub> pretreatment, aldehyde selectivity decreased down to 34.6%. It is also interesting to note that redox pretreatment only affected the selectivity of AuAg samples, as AgAu samples demonstrated similar selectivity for each product after all applied pretreatments.

### 2.3. Comparison of Catalytic and Physicochemical Results

There was no direct correlation between the activity of the samples and the average size of the metal nanoparticles (Figure 2). This is due to the well-reported fact that, in some cases, only gold nanoparticles with sizes below 5 nm showed catalytic activity; the larger particles were simply "spectators" of the process [72–76]. Our previous studies have shown that the active particles are smaller than 2 nm, some of which were undetectable by TEM and XRD methods [63,73]. In addition, in bimetallic samples, it is impossible to discriminate TEM images of Au and Ag clusters. Moreover, it should be taken into account that some of the gold and silver is in the ionic state, and TEM is known to be insensitive to such states.

The UV-vis DRS method (Figure 3) showed that in bimetallic samples, the plasmon signals related to gold nanoparticles are close, but this method did not provide information about the ionic states of the deposited metals, due to the overlap of the absorption of the carrier and modifiers in the region of 200–400 nm.

The observed effects can be explained as follows: in as-prepared samples, a significant part of both metals was in the ionic state, that is, Ag<sup>+</sup>, Au<sup>3+</sup> and Au<sup>+</sup> [39,40,63]. According to the previously reported results, single-charged ions are active sites of low-temperature oxidation of CO and alcohols, while Au<sup>3+</sup> was inactive in the studied processes [22,39,49,50]. This is probably the reason why in the AuAg series of samples, where silver was deposited first, as-prepared catalysts were more active, and subsequent pretreatments led to complete or partial reduction of the ions. In the case of O<sub>2</sub> pretreatment, Ag<sup>+</sup> ions were thermally reduced. In the series of AgAu samples (i.e., gold was deposited first), due to the more complex surface composition (Au<sup>0</sup>, Au<sup>3+</sup>, Au<sup>+</sup>), the effect of pretreatment was contradictory and not so pronounced, because the reduction of Au<sup>3+</sup> to Au<sup>+</sup> increased the activity, while the reduction of Au<sup>+</sup> to Au<sup>0</sup> decreased it. However, the XPS data (Figure 4, Table 1) show that even after treatment in hydrogen at 300 °C, not all ionic states were reduced to Au<sup>0</sup> and Ag<sup>0</sup>, as some of the ions were quite stable due to strong interaction with the support.

In both series of samples, La-modified catalysts were an exception to the general trends. Our previous studies of monometallic Au catalysts and the literature data have shown that  $\text{La}_2\text{O}_3$  is the best promoter of gold catalysts for the oxidation of CO and alcohols [38,39,77,78]. This was explained by the stabilization of the active states of the metal single-charge cations ( $\text{Au}^+$ ). In the case of bimetallic catalysts, similar effects were observed.

#### 2.4. Theoretical Calculations

To confirm our assumptions concerning the reasons for the catalytic activity of samples, we conducted a quantum-chemical simulation of our clusters by the density functional theory (DFT) method.

Quantum-chemical simulations, including calculation of the adsorption energy of octanol on monometallic and bimetallic AuAg clusters containing 10 atoms, were performed to determine the structure of the active site of the AuAg catalysts.

Several models were considered as  $\text{Au}_x\text{Ag}_y$  ( $x + y = 10$ ) clusters with the optimized structures presented in Figure 7: monometallic  $\text{Au}_{10}$  and  $\text{Ag}_{10}$  clusters, bimetallic  $\text{AgAu}_9$  and  $\text{AuAg}_9$  clusters with a low content of heteroatom, bimetallic  $\text{Au}_4\text{Ag}_6$  and  $\text{Ag}_4\text{Au}_6$  clusters with monometallic layers with a metal ratio of 2:3 and 3:2, and a bimetallic  $\text{Au}_5\text{Ag}_5$  cluster with a random arrangement of atoms with a 1:1 metal ratio. To study the charge effect of metal site on the adsorption of octanol, neutral and positively charged clusters were considered. Mono- and bimetallic clusters have a similar 3D structure.

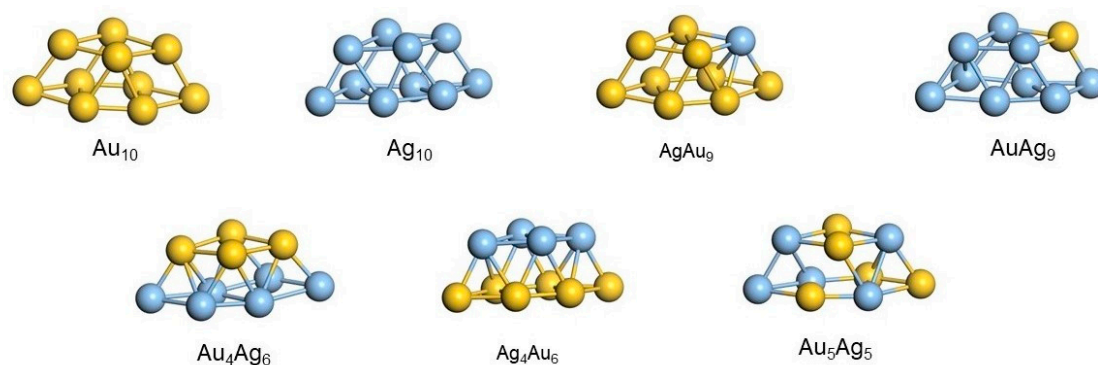


**Figure 7.** Optimized structures of mono- and bimetallic  $\text{Au}_x\text{Ag}_y$  ( $x + y = 10$ ) clusters.

The adsorption of octanol on  $\text{Au}_x\text{Ag}_y^q$  clusters ( $x + y = 10$ , with a charge of  $q = 0$  or  $+1$ ) was simulated through adsorption (1) and (2); the study involved determination of the structure (Figure 8) and energy of  $\text{C}_8\text{H}_{17}\text{OH}\text{-Au}_x\text{Ag}_y^q$  complexes.

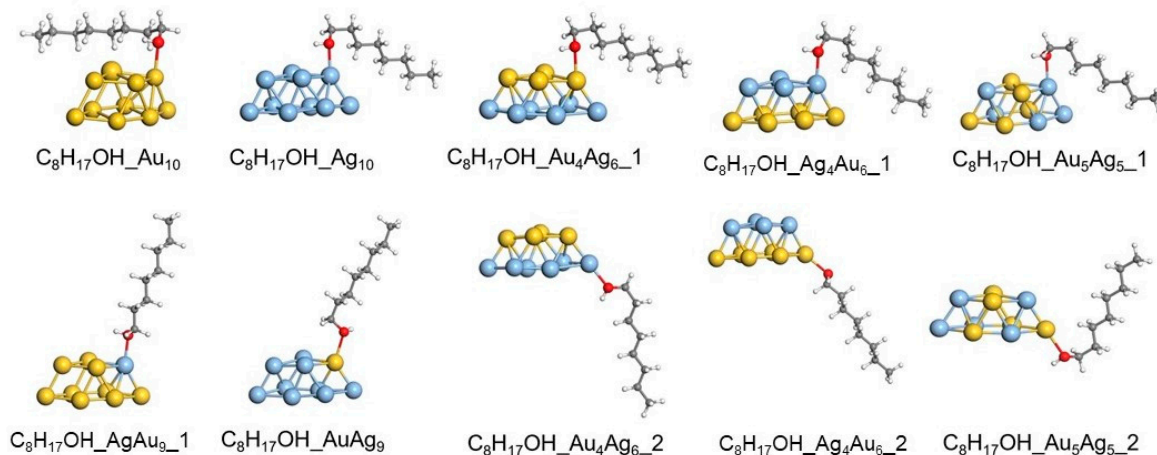


**Figure 8.** Optimized structures of  $\text{C}_8\text{H}_{17}\text{OH}\text{-Au}_x\text{Ag}_y$  ( $x + y = 10$ ) complexes.

The energy of octanol adsorption on  $Au_xAg_y$  ( $x + y = 10$ ) was calculated by Equations (3) and (4), and the results are presented in Table 4. Firstly, we consider the results obtained for the neutral clusters. According to the calculation results, 1-octanol was better adsorbed on  $Au_{10}$  than on  $Ag_{10}$  monometallic clusters: the binding energy of  $C_8H_{17}OH$  with a silver atom in  $Ag_{10}$  was 13 kJ/mol lower than with a gold atom having the same coordination number in  $Au_{10}$ . However, the introduction of even one silver atom into the gold 10-atom cluster (see the results for  $AgAu_9$  in Figure 8) model increased the binding energy of the adsorption of alcohol on the Ag heteroatom up to 47 kJ/mol. In contrast, the introduction of one Au heteroatom into the silver cluster ( $AuAg_9$ ) decreased the activity of gold in the activation of alcohol. It should be noted that  $Au_5Ag_5$  with a random atomic arrangement had lower adsorption energy than the layered  $Au_4Ag_6$  and  $Ag_4Au_6$  clusters.

**Table 4.** Calculated energies of octanol adsorption on  $Au_xAg_y$  ( $x + y = 10$ ) in kJ/mol. Sites of octanol coordination (Au and Ag) are in parentheses.

Charge	$Au_{10}$	$Ag_{10}$	$AgAu_9$	$AuAg_9$	$Au_4Ag_6$	$Ag_4Au_6$	$Au_5Ag_5$
0	−43 (Au)	-	-	−11 (Au)	−26 (Au)	−26 (Au)	−17 (Au)
	-	−30 (Ag)	−47 (Ag)	-	−42 (Ag)	−39 (Ag)	−33 (Ag)
1	−100 (Au)	-	-	−57 (Au)	−73 (Au)	−73 (Au)	−79 (Au)
	-	−73 (Ag)	−87 (Ag)	-	−86 (Ag)	−94 (Ag)	−85 (Ag)

For all considered neutral bimetallic clusters, the silver atom was more active in the adsorption of octanol than the gold atom. This pattern was also preserved for positively charged  $Au_xAg_y^+$ , in which  $C_8H_{17}OH$  adsorbed more strongly than on  $Au_xAg_y$ . Thus, a positive charge in all the considered clusters improved octanol adsorption.

The greatest charge effect was observed for the  $Au_5Ag_5$  cluster with a random arrangement of gold and silver. The calculated  $\Delta E_2$  values were  $-79$  kJ/mol and  $-85$  kJ/mol on the Au and Ag sites, respectively. The same values of  $\Delta E_2$  were obtained for layered  $Au_4Ag_6$  and  $Ag_4Au_6$ . Thus, the arrangement ordering effect on octanol adsorption was blurred in positive bimetallic AuAg clusters.

Thus, DFT/PBE (density functional theory/Perdew–Burke–Eenzerhof) simulation of 1-octanol adsorption on neutral and positively charged  $Au_xAg_y$  clusters containing 10 atoms was performed to reveal the active site of the Au–Ag nanoparticles. Bimetallic clusters with a different content of heteroatoms and different atomic arrangements (random or layer) were considered as models. According to the adsorption energy calculation, the silver atom was more active in the adsorption of  $C_8H_{17}OH$  than the gold atom in all considered neutral bimetallic clusters. The ordered structure of layered gold–silver nanoparticles promoted 1-octanol adsorption as opposed to bimetallic systems with a random atomic arrangement. The adsorption energy of 1-octanol increased for all positively charged  $Au_xAg_y^q$  clusters ( $x + y = 10$ , with a charge of  $q = 0$  or  $+1$ ) compared with the neutral counterparts.

### 3. Materials and Methods

#### 3.1. Catalyst Preparation

$TiO_2$  (45  $m^2 g^{-1}$ , nonporous, 70% anatase and 30% rutile, purity >99.5%; Titania Evonik P25, Degussa GmbH, Essen, Germany) was used as the starting support. Before use,  $TiO_2$  was dried in air at 100 °C for 24 h.

Modification of  $TiO_2$  with metal oxides of Ce, La, Fe or Mg (M) was made by impregnation (2.5  $cm^3/g$ ) with  $3.1 \times 10^{-4}$  M aqueous solutions of  $Ce(NO_3)_3$ ,  $La(NO_3)_3$ ,  $Fe(NO_3)_3$  or  $Mg(NO_3)_2$  (Sigma-Aldrich, St. Louis, MO, USA). The nominal molar ratio Ti/M was 40. The impregnation products were dried at room temperature for 48 h, then at 110 °C for 4 h, and finally calcined at 550 °C for 4 h in static air.

Gold (nominal loading: 4 wt.%) and silver (nominal loading: 2.2 wt.%), which corresponded to 0.56 at.% for both Au and Ag, with different deposition orders (AgAu or

AuAg), were deposited on the supports by deposition–precipitation (DP), following the previously reported procedure [41–44].

The abbreviations used for bimetallic catalysts are as follows: if silver was deposited first and then Au, such samples were denoted as AuAg/M/TiO<sub>2</sub>, while if Au was deposited first and then Ag, the samples were identified as AgAu/M/TiO<sub>2</sub>.

For gold deposition, HAuCl<sub>4</sub> ( $4.2 \times 10^{-3}$  M, Merck, Darmstadt, Germany) and urea (0.42 M, Merck, Darmstadt, Germany) were dissolved in 50 mL of distilled water; the pH of the solution was 2.4. Next, 1 g of M/titania (if gold was supported first) or 1 g of solid Ag/M/TiO<sub>2</sub> (if silver was supported first) was added to this solution following heating to 80 °C for 16 h under stirring. Thereafter, the samples were centrifuged and washed with water. This procedure was repeated 4 times. The samples were then dried under a vacuum for 2 h at 80 °C.

Silver was deposited on doped or undoped titania as follows: 1 g of M/TiO<sub>2</sub> (if silver was supported first) or 1 g of solid Au/M/TiO<sub>2</sub> (if gold was supported first) was added to 54 mL of an aqueous solution containing AgNO<sub>3</sub> ( $4.2 \times 10^{-3}$  M, Merck, Darmstadt, Germany). The solution was heated to 80 °C. The initial pH was ~3, then it was adjusted to 9 by dropwise addition of NaOH (0.5 M, Merck, Darmstadt, Germany), promoting AgOH precipitation on TiO<sub>2</sub> or Au/M/TiO<sub>2</sub>, followed by decomposition to Ag<sub>2</sub>O. The suspension was vigorously stirred for 2 h at 80 °C. The samples were then centrifuged, washed and dried, following the same procedure described for the gold catalysts.

The samples prior to pretreatment are denoted as “as-prepared” catalysts. Hydrogen or oxygen pretreatments (flow rate 300 mL/min, 15% H<sub>2</sub> or O<sub>2</sub> in He, 300 °C for 1 h) were applied to study the effect of sample pretreatment. All materials were stored in a desiccator under a vacuum at room temperature, away from the light.

### 3.2. Characterization of the Samples

All supports and as-prepared catalysts were pretreated in hydrogen at 300 °C for 1 h before characterization by all methods applied in this work.

Catalysts were characterized by X-ray diffraction (XRD) with a Philips XPert PRO diffractometer (Malvern PANalytical Products, Malvern, UK), adsorption–desorption of N<sub>2</sub> at −196 °C on a Micromeritics Tristar 3000 Apparatus (Micromeritics Instrument Corporation, Norcross, GA, USA), energy-dispersive X-ray spectroscopy (EDX) and high-resolution transmission electronic microscopy (HRTEM) using a JEM 2100F (JEOL Ltd., Tokyo, Japan) microscope, ultraviolet–visible diffuse reflectance spectroscopy (UV–vis DRS) with a CARY 300 SCAN (Varian Inc, Palo Alto, CA, USA) spectrophotometer and X-ray photoelectron spectroscopy (XPS), performed on a SPECS GmbH custom (SPECS Surface Nano Analysis GmbH, Berlin, Germany). Further details are presented in [39,40,63].

### 3.3. Theoretical Calculations

The 1-octanol adsorption on Au, Ag and Au–Ag nanoparticles was simulated using the density functional theory PBE [79]. Mono- and bimetallic Au<sub>x</sub>Ag<sub>y</sub><sup>q</sup> clusters (x + y = 10, with a charge of q = 0 or +1) were considered as a model for nanoparticles. The choice of the model is explained by the fact that the Au<sub>10</sub> cluster, which has a 2-layer structure, has been established as an active site of gold nanoparticles deposited on iron oxide in CO oxidation [80].

Octanol adsorption was simulated as follows:



Adsorption of alcohol on low coordinated Au or Ag atoms of Au<sub>x</sub>Ag<sub>y</sub><sup>q</sup> was considered only. The adsorbed structures of ((C<sub>8</sub>H<sub>17</sub>OH)Au<sub>x</sub>Ag<sub>y</sub>) were optimized. The energy of zero

vibrations was taken into account to calculate the total energy of the reagents and products (E). Adsorption energy ( $\Delta E$ ) was calculated as follows:

$$\Delta E_1 = E((C_8H_{17}OH)Au_xAg_y) - E(Au_xAg_y) - E(C_8H_{17}OH) \quad (3)$$

$$\Delta E_2 = E((C_8H_{17}OH)Au_xAg_y^+) - E(Au_xAg_y) - E(C_8H_{17}OH) \quad (4)$$

According to Equations (3) and (4), the large values of  $\Delta E_1$  and  $\Delta E_2$  in the module pointed to high adsorption of octanol on  $Au_xAg_y$ .

All DFT calculations were performed using the PRIRODA program (version 17, Russia) [81] in the Lomonosov supercomputer [82].

### 3.4. Catalytic Tests in 1-Octanol Oxidation

The catalytic properties for n-octanol oxidation were studied using catalyst samples either without treatment or after pretreatment at 300 °C in a H<sub>2</sub> or O<sub>2</sub> atmosphere. Typically, the catalyst sample (substrate/gold (R) = 100 mol/mol) was added to 25 mL of 1-octanol (0.1 M) in *n*-heptane (Supelco, 99%, HPLC grade) as a solvent, in a 4-necked round-bottomed flask equipped with a reflux condenser, an oxygen feed, a thermometer and a septum cap. The reaction mixture was stirred in a batch reactor operated under atmospheric conditions at 80 °C. Oxygen was bubbled through the suspension at a flow rate of 30 mL/min for 6 h. Small aliquots were obtained from the reactor by using nylon syringe filters (pore 0.45 μm), during and at the end of the test for monitoring the reaction progress. The oxidized products were analyzed in a Varian 450 gas chromatograph (Varian Inc, Palo Alto, CA, USA), using a capillary DB wax column (15 m × 0.548 mm, Varian Inc., Palo Alto, CA, USA) and He as the carrier gas.

Alcohol conversion and product selectivity were calculated in terms of moles of C atoms, as detailed in [83]. Carbon balances in all reported data were within 100 ± 3%.

## 4. Conclusions

In the present work, it was revealed that the catalytic, structural and electronic properties of bimetallic Au-Ag catalysts for liquid-phase oxidation of 1-octanol strongly depended on the order in which the metals were deposited on the oxide support. This was confirmed by the effects of pretreatment with hydrogen and oxygen, which significantly decreased the activity of AuAg catalysts (silver was deposited first) and had little effect on the catalytic properties of AgAu samples (gold was deposited first). As silver is more sensitive to redox reactions than gold, such differences may be due to the higher stabilization of silver's electronic states, caused by its preferential interaction with the support, if deposited first. It was revealed that lanthanum oxide is the most effective promoter for AuAg and AgAu catalysts in 1-octanol oxidation. This is consistent with the highest efficiency shown by lanthanum oxide as a promoter for monometallic Ag and Au catalysts in this reaction. The density functional theory method demonstrated that the introduction of even one silver atom into the gold 10-atom cluster model increased the binding energy of the adsorption of alcohol on the Ag heteroatom. In contrast, the introduction of one Au heteroatom into the silver cluster (AuAg<sub>9</sub>) decreased the activity of gold in the activation of alcohol. It should be noted that Au<sub>5</sub>Ag<sub>5</sub> with a random atomic arrangement had lower adsorption energy than the layered Au<sub>4</sub>Ag<sub>6</sub> and Ag<sub>4</sub>Au<sub>6</sub> clusters. The calculations also showed that the adsorption energy of 1-octanol increased for all positively charged Au<sub>x</sub>Ag<sub>y</sub><sup>q</sup> clusters (x + y = 10, with a charge of q = 0 or +1) compared with their neutral counterparts. The obtained results contribute to our understanding of the reaction mechanism and to the search for key parameters for the design of active and selective catalysts for liquid-phase oxidation of 1-octanol, which is a model reaction for the conversion of biomass into chemical products of great industrial impact.

**Supplementary Materials:** The following are available online at <https://www.mdpi.com/article/10.3390/catal11070799/s1>, Table S1: Textural properties of the supports and catalysts, and the EDX content of Au and Ag. Figure S1: Representative HRTEM micrographs of the catalysts.

**Author Contributions:** Conceptualization, Y.K., A.P. and E.K.; methodology, E.P., M.H.F., V.C.C. and S.A.C.C.; software, D.P. and N.N.; validation, Y.K., A.P., N.B. and E.K.; formal analysis, A.P., M.H.F., D.P., N.N. and V.C.C.; investigation, Y.K., E.K., E.P., D.P., N.N. and M.H.F.; resources, A.P., V.C.C., M.H.F. and S.A.C.C.; data curation, Y.K., A.P., E.K., M.H.F., V.C.C. and S.A.C.C.; writing—original draft preparation, Y.K., A.P., E.P. and V.C.C.; writing—review and editing, N.B., V.C.C.; visualization, Y.K., M.H.F., N.B., D.P. and N.N.; supervision, A.P. and E.K.; project administration, A.P.; funding acquisition, A.P. All authors have read and agreed to the published version of the manuscript.

**Funding:** The research was funded by the Tomsk Polytechnic University Development Program “Priority 2030”. This work was also supported by national funds through FCT—Fundação para a Ciência e a Tecnologia, I.P., Portugal, under the Scientific Employment Stimulus—Institutional Call (CEECINST/00102/2018) and partially supported by the Associate Laboratory for Green Chemistry—LAQV, financed by national funds from FCT/MCTES (UIDB/50006/2020 and UIDP/50006/2020), by SevSU Research grant 42-01-09/169/2021-4 and by MINECO project CTQ2017-86170-R (Spain).

**Data Availability Statement:** Data are available upon request.

**Conflicts of Interest:** The authors declare no conflict of interest.

## References

1. Haruta, M. Gold as a Novel Catalyst in the 21st Century: Preparation, Working Mechanism and Applications. *Gold Bull.* **2004**, *37*, 27–36. [[CrossRef](#)]
2. Bond, G.C. Gold: A relatively new catalyst. *Gold Bull.* **2001**, *34*, 117–119. [[CrossRef](#)]
3. Wang, Y.; Zheng, J.M.; Fan, K.N.; Dai, W.L. One-pot solvent-free synthesis of sodium benzoate from the oxidation of benzyl alcohol over novel efficient AuAg/TiO<sub>2</sub> catalysts. *Green Chem.* **2011**, *13*, 1644–1647. [[CrossRef](#)]
4. Bracey, C.L.; Ellis, P.R.; Hutchings, G.J. Application of copper–gold alloys in catalysis: Current status and future perspectives. *Chem. Soc. Rev.* **2009**, *38*, 2231–2243. [[CrossRef](#)] [[PubMed](#)]
5. Liu, X.Y.; Wang, A.Q.; Wang, X.D.; Mou, C.Y.; Zhang, T. Au-Cu Alloy nanoparticles confined in SBA-15 as a highly efficient catalyst for CO oxidation. *Chem. Commun.* **2008**, *27*, 3187–3189. [[CrossRef](#)] [[PubMed](#)]
6. Ji, Y.; Yang, S.; Guo, S.; Song, X.; Ding, B.; Yang, Z. Bimetallic Ag/Au nanoparticles: A low temperature ripening strategy in aqueous solution. *Colloids Surf. A Physicochem. Eng. Aspects* **2010**, *372*, 204–209. [[CrossRef](#)]
7. Lizuka, Y.; Kawamoto, A.; Akita, K.; Date, M.; Tsubota, S.; Okumura, M.; Haruta, M. Effect of Impurity and Pretreatment Conditions on the Catalytic Activity of Au Powder for CO Oxidation. *Catal. Lett.* **2004**, *97*, 203–208.
8. Carbone, L.; Cozzoli, P.D. Colloidal heterostructured nanocrystals: Synthesis and growth mechanisms. *Nanotoday* **2010**, *5*, 449–493. [[CrossRef](#)]
9. Fu, H.; Yang, X.; Jiang, X.; Yu, A. Bimetallic Ag–Au Nanowires: Synthesis, Growth Mechanism, and Catalytic Properties. *Langmuir* **2013**, *29*, 7134–7142. [[CrossRef](#)]
10. Menezes, W.G.; Zielasek, V.; Thiel, K.; Hartwig, A.; Bäumer, M. Effects of particle size, composition, and support on catalytic activity of AuAg nanoparticles prepared in reverse block copolymer micelles as nanoreactors. *J. Catal.* **2013**, *299*, 222–231. [[CrossRef](#)]
11. Wang, A.-Q.; Liu, J.-H.; Lin, S.D.; Lin, T.-S.; Mou, C.-Y. A novel efficient Au-Ag alloy catalyst system: Preparation, activity, and characterization. *J. Catal.* **2005**, *233*, 186–197. [[CrossRef](#)]
12. Qu, Z.; Ke, G.; Wang, Y.; Liu, M.; Jiang, T.; Gao, J. Investigation of factors influencing the catalytic performance of CO oxidation over Au-Ag/SBA-15 catalyst. *Appl. Surf. Sci.* **2013**, *277*, 293–301. [[CrossRef](#)]
13. An, Q.; Yu, M.; Zhang, Y.; Ma, W.; Guo, J.; Wang, C. Fe<sub>3</sub>O<sub>4</sub>@Carbon Microsphere Supported Ag–Au Bimetallic Nanocrystals with the Enhanced Catalytic Activity and Selectivity for the Reduction of Nitroaromatic Compounds. *Phys. Chem. C* **2012**, *116*, 22432–22440. [[CrossRef](#)]
14. Huang, X.; Wang, X.; Wang, X.; Wang, X.; Tan, M.; Ding, W.; Lu, X. P123-stabilized Au-Ag alloy nanoparticles for kinetics of aerobic oxidation of benzyl alcohol in aqueous solution. *J. Catal.* **2013**, *301*, 217–226. [[CrossRef](#)]
15. Cui, Y.; Wang, Y.; Fan, K.; Dai, W.-L. Surface structural evolution of AuAg/TiO<sub>2</sub> catalyst in the transformation of benzyl alcohol to sodium benzoate. *Appl. Surf. Sci.* **2013**, *279*, 391–399. [[CrossRef](#)]
16. Stucchi, M.; Jouve, A.; Villa, A.; Nagy, G.; Németh, M.; Evangelisti, C.; Zanella, R.; Prati, L. Gold-Silver Catalysts: Ruling Factors for Establishing Synergism. *ChemCatChem* **2019**, *11*, 4043–4053. [[CrossRef](#)]
17. Smetana, A.B.; Klabunde, K.J.; Sorensen, C.M.; Ponce, A.A.; Mwale, B. Low-Temperature Metallic Alloying of Copper and Silver Nanoparticles with Gold Nanoparticles through Digestive Ripening. *J. Phys. Chem. B* **2006**, *110*, 2155–2158. [[CrossRef](#)]
18. Alberto Villa, A.; Wang, D.; Sheng Su, D.; Prati, L. New challenges in gold catalysis: Bimetallic systems. *Catal. Sci. Technol.* **2015**, *5*, 55–68.

19. Mertens, P.G.N.; Vandezande, P.; Ye, X.P.; Poelman, H.; Vankelecom, I.F.J.; De Vos, D.E. Recyclable Au<sup>0</sup>, Ag<sup>0</sup> and Au<sup>0</sup>-Ag<sup>0</sup> nanocolloids for the chemoselective hydrogenation of  $\alpha,\beta$ -unsaturated aldehydes and ketones to allylic alcohols. *Appl. Catal. A Gen.* **2009**, *355*, 176–183. [[CrossRef](#)]
20. Savara, A.; Chan-Thaw, C.E.; Sutton, J.E.; Wang, D.; Prati, L.; Villa, A. Molecular Origin of the Selectivity Differences between Palladium and Gold-Palladium in Benzyl Alcohol Oxidation: Different Oxygen Adsorption Properties. *ChemCatChem* **2017**, *9*, 253–257. [[CrossRef](#)]
21. Zheng, J.; Lin, H.; Wang, Y.; Zheng, X.; Duan, X.; Yuan, Y. Efficient low-temperature selective hydrogenation of esters on bimetallic Au-Ag/SBA-15 catalyst. *J. Catal.* **2013**, *297*, 110–118. [[CrossRef](#)]
22. Kolobova, E.; Pestryakov, A.; Shemeryankina, A.; Kotolevich, Y.; Martynyuk, O.; Tiznado Vazquez, H.J.; Bogdanchikova, N. Formation of silver active states in Ag/ZSM-5 catalysts for CO oxidation. *Fuel* **2014**, *138*, 65–71. [[CrossRef](#)]
23. Kolobova, E.N.; Pestryakov, A.N.; Bogdanchikova, N.; Cortés Corberán, V. Silver catalysts for liquid-phase oxidation of alcohols in green chemistry: Challenges and outlook. *Catal. Today* **2019**, *333*, 81–88. [[CrossRef](#)]
24. Kolobova, E.; Mäki-Arvela, P.; Grigoreva, A.; Pakrieva, E.; Carabineiro, S.A.C.; Peltonen, J.; Kazantsev, S.; Bogdanchikova, N.; Pestryakov, A.; Murzin, D.Y. Catalytic oxidative transformation of betulin to its valuable oxo-derivatives over gold supported catalysts: Effect of support nature. *Catal. Today* **2021**, *367*, 95–110. [[CrossRef](#)]
25. Mott, D.M.; Anh, D.T.N.; Singh, P.; Shankar, C.; Maenosono, S. Electronic transfer as a route to increase the chemical stability in gold and silver core-shell nanoparticles. *Adv. Colloid Interface Sci.* **2012**, *185–186*, 14–33. [[CrossRef](#)]
26. Nakatsujii, H.; Hu, Z.M.; Nakai, H.; Ikeda, K. Activation of O<sub>2</sub> on Cu, Ag, and Au surfaces for the epoxidation of ethylene: Dipped adcluster model study. *Surf. Sci.* **1997**, *387*, 328–341. [[CrossRef](#)]
27. Sandell, A.; Bennich, P.; Nilsson, A.; Hernnäs, B.; Björneholm, O.; Mårtensson, N. Chemisorption of CO on Cu(100), Ag(110) and Au(110). *Surf. Sci.* **1994**, *310*, 16–26. [[CrossRef](#)]
28. Bokhimi, X.; Zanella, R.; Maturano, V.; Morales, A. Nanocrystalline Ag, and Au-Ag alloys supported on titania for CO oxidation reaction. *Mat. Chem. Phys.* **2013**, *138*, 490–499. [[CrossRef](#)]
29. Liu, X.Y.; Li, Y.N.; Lee, J.W.; Hong, C.Y.; Mou, C.Y.; Jang, B.W.L. Selective hydrogenation of acetylene in excess ethylene over SiO<sub>2</sub> supported Au-Ag bimetallic catalyst. *Appl. Catal. A Gen.* **2012**, *439–440*, 8–14. [[CrossRef](#)]
30. Doherty, R.P.; Krafft, J.-M.; Methivier, C.; Casale, S.; Remita, H.; Louis, C.; Thomas, C. On the promoting effect of Au on CO oxidation kinetics of Au-Pt bimetallic nanoparticles supported on SiO<sub>2</sub>: An electronic effect? *J. Catal.* **2012**, *287*, 102–113. [[CrossRef](#)]
31. Yang, X.; Chen, D.; Liao, S.J.; Song, H.Y.; Li, Y.W.; Fu, Z.Y.; Su, Y.L. High-performance Pd-Au bimetallic catalyst with mesoporous silica nanoparticles as support and its catalysis of cinnamaldehyde hydrogenation. *J. Catal.* **2012**, *291*, 36–43. [[CrossRef](#)]
32. Liu, J.H.; Wang, A.Q.; Chi, Y.S.; Lin, H.P.; Mou, C.Y. Platinum Monolayer on Nonnoble Metal-Noble Metal Core-Shell Nanoparticle Electrocatalysts for O<sub>2</sub> Reduction. *J. Phys. Chem. B* **2005**, *109*, 22701–22704.
33. Liu, J.H.; Wang, A.Q.; Chi, Y.S.; Lin, H.P.; Mou, C.Y. Synergistic Effect in an Au-Ag Alloy Nanocatalyst: CO Oxidation. *J. Phys. Chem. B* **2005**, *109*, 40–43. [[CrossRef](#)]
34. Wang, A.-Q.; Hsieh, Y.-P.; Chen, Y.-F.; Mou, C.-Y. Au-Ag alloy nanoparticle as catalyst for CO oxidation: Effect of Si/Al ratio of mesoporous support. *J. Catal.* **2006**, *237*, 197–206. [[CrossRef](#)]
35. Sandoval, A.; Aguilar, A.; Louis, C.; Traverse, A.; Zanella, R. Bimetallic Au-Ag/TiO<sub>2</sub> catalyst prepared by deposition-precipitation: High activity and stability in CO oxidation. *J. Catal.* **2011**, *281*, 40–49. [[CrossRef](#)]
36. Wittstock, A.; Zielasek, V.; Biener, J.; Friend, C.M.; Baumer, M. Nanoporous gold catalysts for selective gas-phase oxidative coupling of methanol at low temperature. *Science* **2010**, *327*, 319–322. [[CrossRef](#)]
37. Moskaleva, L.V.; Rohe, S.; Wittstock, A.; Zielasek, V.; Kluner, T.; Neyman, K.M.; Baumer, M. Silver residues as a possible key to a remarkable oxidative catalytic activity of nanoporous gold. *Phys. Chem. Chem. Phys.* **2011**, *13*, 4529–4539. [[CrossRef](#)]
38. Cortés Corberán, V.; González-Pérez, M.E.; Martínez-González, S.; Gómez-Avilés, A. Green oxidation of fatty alcohols: Challenges and opportunities. *Appl. Catal. A Gen.* **2014**, *474*, 211–223. [[CrossRef](#)]
39. Kotolevich, Y.; Kolobova, E.; Khramov, E.; Farías, M.H.; Zubavichus, Y.; Tiznado, H.; Martínez-González, S.; Cortés Corberán, V.; Mota-Morales, J.D.; Pestryakov, A.; et al. n-Octanol oxidation on Au/TiO<sub>2</sub> catalysts promoted with La and Ce oxides. *Molecular Catal.* **2017**, *14*, 1–10.
40. Kotolevich, Y.; Kolobova, E.; Mamontov, G.; Khramov, E.; Cabrera Ortega, J.E.; Tiznado, H.; Farías, M.H.; Bogdanchikova, N.; Zubavichus, Y.; Cortés Corberán, V.; et al. Au/TiO<sub>2</sub> catalysts promoted with Fe and Mg for selective n-octanol oxidation under mild conditions. *Catal. Today* **2016**, *278*, 104–112. [[CrossRef](#)]
41. Zanella, R.; Giorgio, S.; Henry, C.R.; Louis, C. Alternative Methods for the Preparation of Gold Nanoparticles Supported on TiO<sub>2</sub>. *J. Phys. Chem. B* **2002**, *106*, 7634–7642. [[CrossRef](#)]
42. Zanella, R.; Delannoy, L.; Louis, C. Mechanism of deposition of gold precursors onto TiO<sub>2</sub> during the preparation by cation adsorption and deposition-precipitation with NaOH and urea. *Appl. Catal. A Gen.* **2005**, *291*, 62–72. [[CrossRef](#)]
43. Zanella, R.; Louis, C. Influence of the conditions of thermal treatments and of storage on the size of the gold particles in Au/TiO<sub>2</sub> samples. *Catal. Today* **2005**, *107–108*, 768–777. [[CrossRef](#)]
44. Kotolevich, Y.; Kolobova, E.; Cabrera Ortega, J.E.; Khramov, E.; Pakrieva, E.; Zubavichus, Y.; Cortés Corberán, V.; Zanella, R.; Bogdanchikova, N.; Pestryakov, A. Gold and Silver Catalysts for Liquid Phase n-Octanol Oxidation: Effect of Promoters. *Curr. Org. Synth.* **2017**, *14*, 322–331.

45. Rojluechai, S.; Chavadej, S.; Schwank, J.W.; Meeyoo, V. Catalytic activity of ethylene oxidation over Au, Ag and Au-Ag catalysts: Support effect. *Catal. Comm.* **2007**, *8*, 57–64. [[CrossRef](#)]
46. Zhang, Q.B.; Lee, J.Y.; Yang, J.; Boothroyd, C.; Zhang, J.X. Size and composition tunable Ag–Au alloy nanoparticles by replacement reactions. *Nanotechnol.* **2007**, *18*, 245605–245612. [[CrossRef](#)]
47. Mallin, M.P.; Murphy, C. Solution-phase synthesis of sub-10 nm Au-Ag alloy nanoparticles. *J. Nano Lett.* **2002**, *2*, 1235–1237. [[CrossRef](#)]
48. Liu, X.; Wang, A.; Li, L.; Zhang, T.; Mou, C.-Y.; Lee, J.-F. Synthesis of Au-Ag alloy nanoparticles supported on silica gel via galvanic replacement reaction. *Prog. Nat. Sci. Mat. Int.* **2013**, *23*, 317–325. [[CrossRef](#)]
49. Tuzovskaya, I.V.; Simakov, A.V.; Pestryakov, A.N.; Bogdanchikova, N.E.; Gurin, V.V.; Farías, M.H.; Tiznado, H.J.; Avalos, M. Co-existence of various active gold species in Au-mordenite catalyst for CO oxidation. *Catal. Comm.* **2007**, *8*, 977–980. [[CrossRef](#)]
50. Rolima, W.R.; Pelegrino, M.T.; Lima, B.A.; Ferraza, L.S.; Costa, F.N.; Bernardes, J.S.; Rodrigues, T.; Brocchi, M.; Seabra, A.B. Green tea extract mediated biogenic synthesis of silver nanoparticles: Characterization, cytotoxicity evaluation and antibacterial activity. *Appl. Surf. Sci.* **2019**, *463*, 66–74. [[CrossRef](#)]
51. Riaz, M.; Mutreja, V.; Sareen, S. Exceptional antibacterial and cytotoxic potency of monodisperse greener AgNPs prepared under optimized pH and temperature. *Sci. Rep.* **2021**, *11*, 2866. [[CrossRef](#)]
52. Aspromonte, S.G.; Serra, R.M.; Miró, E.E.; Boix, A.V. AgNaMordenite catalysts for hydrocarbon adsorption and deNO<sub>x</sub> processes. *Appl. Catal. A Gen.* **2011**, *407*, 134–144. [[CrossRef](#)]
53. Lysenko, V.S.; Mal'nev, A.F. Optical characteristics of metal blacks. *J. Appl. Spectrosc.* **1969**, *10*, 838–845. [[CrossRef](#)]
54. Rodríguez-Iznaga, I.; Petranovskii, V.; Castellón-Barraza, F.; Concepción-Rosabal, B. Copper-Silver Bimetallic System on Natural Clinoptilolite: Thermal Reduction of Cu<sup>2+</sup> and Ag<sup>+</sup> Exchanged. *J. Nanosci. Nanotechnol.* **2011**, *11*, 5580–5586. [[CrossRef](#)]
55. Gurin, V.S.; Bogdanchikova, N.E.; Petranovskii, V.P. Metal clusters and nanoparticles assembled in zeolites: An example of stable materials with controllable particle size. *Mater. Sci. Eng. C* **2002**, *19*, 327–331. [[CrossRef](#)]
56. Chen, L.X.; Lv, J.J.; Wang, A.J.; Huang, H.; Feng, J.J. One-step wet-chemical synthesis of gold nanoflower chains as highly active surface-enhanced Raman scattering substrates. *Sens. Actuators B* **2016**, *222*, 937–944. [[CrossRef](#)]
57. Zimbone, M.; Calcagno, L.; Messina, G.; Baeri, P.; Compagnini, G. Dynamic light scattering and UV–vis spectroscopy of gold nanoparticles solution. *Mater. Lett.* **2011**, *65*, 2906–2909. [[CrossRef](#)]
58. Fernández-Blanco, C.; Colina, A.; Heras, A.; Ruiz, V.; López-Palacios, J. Multipulse strategies for the electrosynthesis of gold nanoparticles studied by UV/Vis spectroelectrochemistry. *Electrochem. Comm.* **2012**, *18*, 8–11. [[CrossRef](#)]
59. Cybula, A.; Priebe, J.B.; Pohl, M.-M.; Sobczak, J.W.; Schneider, M.; Zielińska-Jurek, A.; Brückner, A.; Zaleska, A. The effect of calcination temperature on structure and photocatalytic properties of Au/Pd nanoparticles supported on TiO<sub>2</sub>. *Appl. Catal. B Environ.* **2014**, *152–153*, 202–211. [[CrossRef](#)]
60. Pestryakov, A.N.; Bogdanchikova, N.; Simakov, A.; Tuzovskaya, I.; Jentoft, F.; Farias, M.; Díaz, A. Catalytically active gold clusters and nanoparticles for CO oxidation. *Surf. Sci.* **2007**, *601*, 3792–3795. [[CrossRef](#)]
61. Yang, G.; Fu, X.; Zhou, J. Dielectric properties of the silver–copper alloy films deposited by magnetron sputtering. *J. Opt. Soc. Am. B* **2013**, *30*, 282–287. [[CrossRef](#)]
62. Gurgul, J.; Łatka, K.; Hnat, I.; Rynkowski, J.; Dzwigaj, S. Identification of iron species in FeSiBEA by DR UV-vis, XPS and Mössbauer spectroscopy: Influence of Fe content. *Micropor. Mesopor. Mater.* **2013**, *168*, 1–6. [[CrossRef](#)]
63. Kotolevich, Y.; Kolobova, E.; Khramov, E.; Cabrera Ortega, J.E.; Farías, M.H.; Zubavichus, Y.; Zanella, R.; Mota-Morales, J.D.; Pestryakov, A.; Bogdanchikova, N.; et al. Identification of subnanometric Ag species, their interaction with supports and role in catalytic CO oxidation. *Molecules* **2016**, *21*, 532. [[CrossRef](#)] [[PubMed](#)]
64. Feldheim, D.L.; Foss, C.A. *Metal Nanoparticles: Synthesis, Characterization and Applications*; Basel Marcel Dekker Inc.: New York, NY, USA, 2002; p. 338.
65. Costa, V.V.; Estrada, M.; Demidova, Y.; Prosvirin, I.; Kriventsov, V.; Cotta, R.F.; Gusevskaya, E.V. Gold nanoparticles supported on magnesium oxide as catalysts for the aerobic oxidation of alcohols under alkali-free conditions. *J. Catal.* **2012**, *292*, 148–156. [[CrossRef](#)]
66. Feng, R.; Li, M.; Liu, J. Synthesis of core–shell Au@Pt nanoparticles supported on Vulcan XC-72 carbon and their electrocatalytic activities for methanol oxidation. *Coll. Surf. A* **2012**, *406*, 6–12. [[CrossRef](#)]
67. Guzmán, C.; del Ángel, G.; Gómez, R.; Galindo-Hernández, F.; Ángeles-Chavez, C. Degradation of the herbicide 2, 4-dichlorophenoxyacetic acid over Au/TiO<sub>2</sub>-CeO<sub>2</sub> photocatalysts: Effect of the CeO<sub>2</sub> content on the photoactivity. *Catal. Today* **2011**, *166*, 146–151. [[CrossRef](#)]
68. Galindo-Hernández, F.; Wang, R.; Gómez, J.A.; Bokhimi, X.; Lartundo, L.; Mantilla, A. Structural modifications in Au/Al<sub>2</sub>O<sub>3</sub>-CeO<sub>2</sub> mixed oxides as a function of Ce<sup>4+</sup> content and its effects in the mineralization of the herbicide diuron. *J. Photochem. Photobiol. A Chem.* **2012**, *243*, 23–32. [[CrossRef](#)]
69. Rtimi, S.; Baghriche, O.; Sanjines, R.; Pulgarin, C.; Bensimon, M.; Kiwi, J. TiON and TiON-Ag sputtered surfaces leading to bacterial inactivation under indoor actinic light. *J. Photochem. Photobiol. A Chem.* **2013**, *256*, 52–63. [[CrossRef](#)]
70. Mejia, I.M.; Marín, M.; Sanjines, R.; Pulgarin, E.; Mielczarski, C.; Mielczarski, J.; Kiwi, L. Magnetron-sputtered Ag-modified cotton textiles active in the inactivation of airborne bacteria. *ACS Appl. Mater. Interfaces* **2010**, *2*, 230–235.
71. Wagner, C.D.; Riggs, M.; Davis, E.; Müllenberg, G. *Handbook of X-ray Photoelectron Spectroscopy*; Perkin-Elmer Corporation Physical Electronics Division: Eden Prairie, MN, USA, 1979; pp. 1–190.

72. Shekhar, M.; Wang, J.; Lee, W.-S.; Williams, W.D.; Min Kim, S.; Stach, E.A.; Miller, J.T.; Delgass, W.N.; Ribeiro, F.H. Size and Support Effects for the Water-Gas Shift Catalysis over Gold Nanoparticles Supported on Model Al<sub>2</sub>O<sub>3</sub> and TiO<sub>2</sub>. *J. Am. Chem. Soc.* **2012**, *134*, 4700–4708. [[CrossRef](#)]
73. Martynyuk, O.; Kotolevich, Y.; Vélez, R.; Cabrera Ortega, J.E.; Tiznado, H.; Zepeda Partida, T.; Mota Morales, J.D.; Pestryakov, A.; Bogdanchikova, N. On the high sensitivity of the electronic states of 1 nm gold particles to pretreatments and modifiers. *Molecules* **2016**, *21*, 432. [[CrossRef](#)]
74. Allard, L.F.; Flytzani-Stephanopoulos, M.; Overbury, S.H. Behavior of Au Species in Au/Fe<sub>2</sub>O<sub>3</sub> Catalysts Characterized by Novel in Situ Heating Techniques and Aberration-Corrected STEM Imaging. *Microsc. Microanal.* **2010**, *16*, 375–385. [[CrossRef](#)] [[PubMed](#)]
75. Lessard, J.D.; Valsamakis, I.; Flytzani-Stephanopoulos, M. Novel Au/La<sub>2</sub>O<sub>3</sub> and Au/La<sub>2</sub>O<sub>2</sub>SO<sub>4</sub> catalysts for the water–gas shift reaction prepared via an anion adsorption method. *Chem. Comm.* **2012**, *48*, 4857–4859. [[CrossRef](#)]
76. Flytzani-Stephanopoulos, M.; Gates, B.C. Atomically Dispersed Supported Metal Catalysts. *Ann. Rev. Chem. Biomol. Eng.* **2012**, *3*, 545–574. [[CrossRef](#)]
77. Kolobova, E.; Kotolevich, Y.; Pakrieva, E.; Mamontov, G.; Farías, M.H.; Bogdanchikova, N.; Cortés Corberán, V.; Pestryakov, A. Causes of activation and deactivation of modified nanogold catalysts during prolonged storage and redox treatments. *Molecules* **2016**, *21*, 486. [[CrossRef](#)] [[PubMed](#)]
78. Sun, X.; Su, H.; Lin, Q.; Han, C.; Zheng, Y.; Sun, L.; Qi, C. Au/Cu-Fe-La-Al<sub>2</sub>O<sub>3</sub>: A highly active, selective and stable catalysts for preferential oxidation of carbon monoxide. *App. Catal. A Gen.* **2016**, *527*, 19–29. [[CrossRef](#)]
79. Perdew, J.P.; Burke, K.; Ernzerhof, M. Generalized Gradient Approximation Made Simple. *Phys. Rev. Lett.* **1996**, *77*, 3865–3868. [[CrossRef](#)]
80. Herzing, A.A.; Kiely, C.J.; Carley, A.F.; Landon, P.; Hutchings, G.J. Identification of active gold nanoclusters on iron oxide supports for CO oxidation. *Science* **2008**, *321*, 1331–1335. [[CrossRef](#)]
81. Laikov, D.N.; Ustynyuk, Y.A. PRIRODA-04: A Quantum-Chemical Program Suite. New possibilities in the study of molecular systems with the application of parallel computing. *Russ. Chem. Bull.* **2005**, *54*, 820–826. [[CrossRef](#)]
82. Sadovnichy, V.; Tikhonravov, A.; Voevodin, V.; Opanasenko, V. *Contemporary High Performance Computing: From Petascale Toward Exascale*; CRC Press: Boca Raton, FL, USA, 2013; pp. 283–307.
83. Pakrieva, E.; Kolobova, E.; Kotolevich, Y.; Pascual, L.; Carabineiro, S.A.C.; Kharlanov, A.N.; Pichugina, D.; Nikitina, N.; German, D.; Zepeda Partida, T.A.; et al. Effect of gold electronic state on the catalytic performance of nano gold catalysts in n-octanol oxidation. *Nanomaterials* **2020**, *10*, 880. [[CrossRef](#)]